Research Article | Vol. 29, No. 4 / 15 February 2021 / Optics Express 5677

Optics EXPRESS

Tailor-made unitary operations using dielectric metasurfaces

MING KANG,[1,2,3] KAI MING LAU,[1,3] TSZ KIT YUNG,[1] SHENGWANG DU,[1] WING YIM TAM,[1] AND JENSEN LI[1,*]

[1]*Department of Physics, Hong Kong University of Science and Technology, Clear Water Bay, Hong Kong, China*
[2]*College of Physics and Materials Science, Tianjin Normal University, Tianjin 300387, China*
[3]*These authors contributed equally to this paper.*
[*]*jensenli@ust.hk*

Abstract: Qubit operation belonging to unitary transformation is the fundamental operation to realize quantum computing and information processing. Here, we show that the complex and flexible light-matter interaction between dielectric metasurfaces and incident light can be used to perform arbitrary U(2) operations. By incorporating both coherent spatial-mode operation together with two polarizations on a single metasurface, we further extend the discussion to single-photon two-qubit U(4) operations. We believe the efficient usage of metasurfaces as a potential compact platform can simplify optical qubit operation from bulky systems into conceptually subwavelength elements.

1. Introduction

Quantum computing and information processing have drawn a lot of interests in the past decade due to the potential speedup over their classical counterparts. Mathematically, an overall quantum operation can be regarded as a series of unitary transformations on the input quantum qubits in constructing a quantum network. There exist many physical systems to realize quantum computing, such as ion traps, Josephson junctions, and nitrogen-vacancy centers, etc. [1]. Among these physical systems, linear optics scheme is appealing because the quantum information carrier is the photon, which is potentially free from decoherence [2,3]. When applying quantum computing on the input photon, the fundamental qubit is usually prepared by single photon in two orthogonal modes or in two polarization channels. To generate the desired evolutions in quantum information processing, each corresponding qubit operation is implemented by some simple optical elements or their combinations, such as beam splitters, phase shifters, and wave plates [4,5]. One-qubit operation belongs to the class of U(2) transformations which have been theoretically discussed and experimentally realized by a combination of these elements [2–6] However, the physical implementation using traditional linear optical elements seem to be bulky and difficult to be integrated to miniaturize the physical system, a potential simplification of the current optics implementation is highly desired.

On the other hand, metasurfaces, a single or multiple layers of metamaterial structures, allow a flat and compact implementation for miniaturizing different optical elements in the classical optical regime [7,8]. Based on the rich degrees of freedom in fabricating any tailor-made and resonating metamaterial structures, they have been applied to different scenarios requiring complicated degrees of freedom, including holograms [9,10], optical flat lens [11,12], Stokes polarimeters [13–15], and analog computation [16–18]. Specifically, metamaterials have been used to perform information or image processing. By pixelating metamaterial into a discrete set of structures, these "digital metamaterials" can be further used to perform different mathematical operations, such as Fourier transform and differentiation [15–22]. Extending to the quantum optical regime, metasurfaces can be useful to substitute conventional linear optical elements

#411467 https://doi.org/10.1364/OE.411467
Journal © 2021 Received 1 Oct 2020; revised 28 Dec 2020; accepted 28 Dec 2020; published 8 Feb 2021

Optics EXPRESS

in either deterministic schemes [23,24] or probabilistic schemes [25] with post-selection for quantum information processing. The complexity embedded with metasurfaces may allow future integration of quantum optical elements, again based on tailor-made resonances and the manipulation of constitutive parameters. Furthermore, it has been suggested in both theory and experiments that metasurfaces are able to achieve fundamental quantum entanglement and quantum interference [26–33]. It is therefore plausible to ask how metasurfaces can be generally used to perform quantum operations, allowing quantum optical schemes to be simplified. To answer this question, it is unavoidable to ask how metasurfaces can be designed to perform a tailor-made unitary operation, which is the common language in a quantum operation.

In this paper, we propose a metasurface platform capable of realizing arbitrary U(2) operations, which may make the general qubit operation migrate from bulky optical systems into conceptually subwavelength elements. Designated unitary transformations can be obtained by varying the geometric parameters of a single metasurface replacing the combination of a beam splitter and a phase shifter [4]. By considering two orthogonal polarizations impinging on a metasurface, we also explore single-photon two-qubit U(4) operations.

2. Theoretical and numerical demonstration

Any U(2) transformations can be performed optically by using one beam splitter and two phase shifters with 2 ports, as shown in Fig. 1(a). In general, for a U(N) transformation, one can decompose into a network of $N(N-1)/2$ sets of U(2) elements with N input and output ports [4]. To simplify this bulky optical implementation, we consider a metasurface with oblique incidence. It can be described by a scattering matrix $\mathbf{S}$ relating two input to two output beams/ports, with the definitions of the ports and polarizations shown in Fig. 1(a). To start with, we demonstrate the designing principle in U(2) for simplicity. In order to suppress polarization conversion, the metasurface has a (mirror) $\mathbf{M}_y$-symmetry and we consider only the vertical polarization ($\mathbf{E}$-field along y) at the moment. The logical states $|0\rangle$ and $|1\rangle$ correspond to the two ports, i.e. a dual-rail qubit. An unitary operation on such a qubit corresponds to an unitary matrix $\mathbf{S}$, i.e. $\mathbf{S}\mathbf{S}^{\dagger} = \mathbf{I}$, which can be fulfilled by a dielectric metasurface with time-reversal symmetry and negligible loss. Two-beam incidence on metasurfaces has already been used for coherent control of absorption and polarization at normal incidence [34,35]. Here, an oblique incidence on both sides is necessary to have different transmission/reflection phases for the two beams in constructing an arbitrary qubit unitary operation. In general for passive optical multiport, the scattering matrix relates the input and output mode operators in the same way to relate the input and output mode functions [36], as a 2×2 unitary matrix written as

$$\mathbf{S} = \begin{pmatrix} t_{11} & r_{12} \\ r_{21} & t_{22} \end{pmatrix} = e^{\frac{i\varphi}{2}} \begin{pmatrix} \sqrt{1-|r|^2}\, e^{\frac{i\Delta\varphi_t}{2}} & |r| e^{-\frac{i(\Delta\varphi_r+\pi)}{2}} \\ |r| e^{\frac{i(\Delta\varphi_r-\pi)}{2}} & \sqrt{1-|r|^2}\, e^{-\frac{i\Delta\varphi_t}{2}} \end{pmatrix} = e^{\frac{i\varphi}{2}} \mathbf{U}, \tag{1}$$

where $t(r)$ is the complex transmission (reflection) coefficient for the two ports in reference to the middle-plane ($z = 0$) of the metasurfaces. We also define $\varphi = Arg(t_{11}) + Arg(t_{22}) = Arg(r_{21}) + Arg(r_{12}) + \pi$ as the global phase, $\Delta\varphi_t = Arg(t_{11}) - Arg(t_{22})$ and $\Delta\varphi_r = Arg(r_{21}) - Arg(r_{12})$ as the phase difference between the transmission coefficients and reflection coefficients respectively. We also define matrix $\mathbf{U}$ without the global phase factor $e^{\frac{i\varphi}{2}}$ such that $\mathrm{Det}(\mathbf{U}) = 1$. For optical measurements, the global phase is not important, as it is only contributed by the distance between source and detector. This allows us to just consider the SU(2) transformation described by three real numbers: reflection amplitude $|r|$, transmission ($\Delta\varphi_t$) and reflection phase differences ($\Delta\varphi_r$). We note that the transmission phases for the two input ports can be different in the case of oblique instead of normal incidence.

As a starting point, we first construct $\mathbf{S} \propto \boldsymbol{\sigma}_z$ as a comparatively simple example. Oblique incidence is set on both sides at 45 degree with vertical polarization and the unit cell (periodic in

Optics EXPRESS

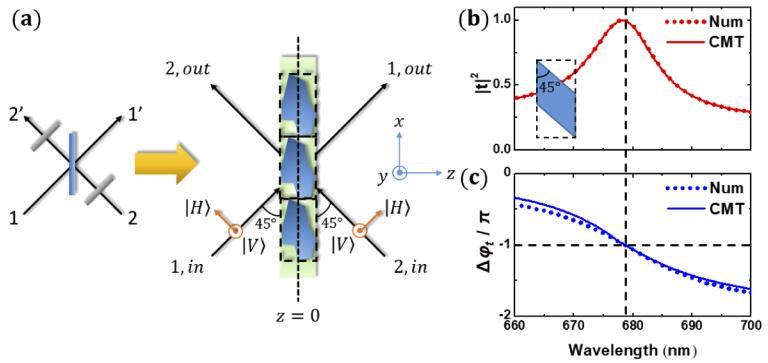

Fig. 1. Metasurface for arbitrary U(2) operation and an example of scattering matrix $\mathbf{S} = \sigma_z$ with unequal transmission. (a) Arbitrary U(2) operation can be implemented by 1 beam splitter and 2 phase shifters, here we replace by single metasurface to simplify the optical setup. (b, c) A parallelogram design to construct unequal transmission of 1 and −1. The numerical simulation (dotted line) and CMT fitted (solid line) both show the transmission amplitude and phase difference achieved the desired value 1 and $-\pi$ at resonance. Structure parameters: dielectric ($\varepsilon_r = 12$) parallelogram at 45 degrees with thickness 84 nm, length 156 nm and lattice constant 240 nm.

x with infinite length in y) is displayed in the inset of Fig. 1(b) (Si parallelogram, with details in caption). The design breaks both $\mathbf{M}_x$ and $\mathbf{M}_z$ symmetries, allowing $t_{11} \neq t_{22} (\Delta\varphi_t \neq 0)$ but retains inversion symmetry $\mathbf{P}$ to have $r_{21} = r_{12}$ ($\Delta\varphi_r = 0$). The unitary scattering matrix is then obtained by full-wave simulation using COMSOL Multiphysics. As shown in the Fig. 1(b) and (c), a resonance is used to achieve zero reflection amplitudes ($|r| = 0$) while the transmission amplitudes for the two input ports stay at one with π-phase difference ($\Delta\varphi_t = -\pi$), at the operational wavelength 678 nm in our current case. To further understand the resonance, a coupled mode theory (CMT) [37,38] is used to capture its essential feature:

$$\frac{dq}{dt} = (-if_0 - \gamma_t)q + \begin{pmatrix} d_1 & d_2 \end{pmatrix} \begin{pmatrix} s_{1,\text{in}} \\ s_{2,\text{in}} \end{pmatrix}, \quad \begin{pmatrix} s_{1,out} \\ s_{2,out} \end{pmatrix} = e^{i\varphi_0} \begin{pmatrix} t_0 & ir_0 \\ ir_0 & t_0 \end{pmatrix} \begin{pmatrix} s_{1,\text{in}} \\ s_{2,\text{in}} \end{pmatrix} + q \begin{pmatrix} d_1 \\ d_2 \end{pmatrix}. \tag{2}$$

The resonant mode having complex amplitude q is described by the resonant frequency f_0, the total scattering decay rate γ_t, and the coupling between the port 1(2) with the resonant mode $d_{1,2} = \sqrt{\gamma_{1,2}} e^{i\varphi_{1,2}}$. The model is established to satisfy $r_{21} = r_{12}$ and the resonance is excited with respect to a reference scattering matrix with coefficients t_0, r_0, global phase φ_0 (satisfying $r_0^2 + t_0^2 = 1$), equivalently represented by a homogeneous dielectric slab of refractive index n_{eff} and thickness h_{eff} [38]. $s_{1(2),\,\text{in(out)}}$ is the incident (output) amplitude from the port 1(2). According to the energy conservation and time reversal symmetry with inversion symmetry, we have $|d_1|^2 + |d_2|^2 = \gamma_1 + \gamma_2 = 2\gamma_t$ and $\gamma_{2,1}/\gamma_{1,2} = 1 + 2(t_0/r_0)^2 + 2(t_0/r_0^2)\cos\delta_{1,2}$, where $\delta_{1,2} = \varphi_0 - 2\varphi_{1,2}$. The two conditions coincide with conventional CMT except that we have to swap the role of r and t to guarantee $r_{21} = r_{12}$ instead of $t_{11} = t_{22}$ [39,40]. Thus, the reflection intensity is

$$R = \frac{\left[r_0(f - f_0) - \sqrt{\gamma_1\gamma_2 - r_0^2\gamma_t^2}\right]^2}{(f - f_0)^2 + \gamma_t^2}. \tag{3}$$

Fitting the reflection intensity according to the CMT, we obtain the resonant mode parameters $f_0 = 442.26$THz, $\gamma_1 = 6.42$THz, $\gamma_2 = 2.21$THz and the background parameters $n_{\text{eff}} = 3.25$ and $h_{\text{eff}} = 73.0$ nm. From the fitting transmission intensity $T = 1 - R$, the transmission difference

Optics EXPRESS

between the two ports is $|t_{11} - t_{22}|^2 = (\gamma_1 - \gamma_2)^2/\{t_0^2[(f - f_0)^2 + \gamma_t^2]\}$. As the phase difference is $\Delta\varphi_t = -2\sin^{-1}\left(|t_{11} - t_{22}|/\left(2\sqrt{T}\right)\right)$, which should be $-\pi$ for our designed metasurface (Fig. 1(b)), we need to achieve the maximum of the difference $|t_{11} - t_{22}| = 2$ at resonant frequency, which further requires $\gamma_1\gamma_2 = r_0^2\gamma_t^2$. Around the resonance, we find good agreement between the numerical and CMT results (Fig. 1(b) and (c)). Based on the CMT, $\Delta\varphi_t$ is mainly from asymmetric scattering coupling of a resonant mode, while away from resonance, the structure can be approximated by a homogenous dielectric slab with effective refractive index and thickness similar to the original structure.

As the global phase φ carries no physical importance, the general SU(2) scattering matrix is written as

$$\mathbf{U} = u_0\mathbf{I} - i\boldsymbol{\sigma}\cdot\mathbf{u}, \tag{4}$$

where $\boldsymbol{\sigma}_x, \boldsymbol{\sigma}_y, \boldsymbol{\sigma}_z$ are the Pauli matrices and $\mathbf{u} = (u_1, u_2, u_3)$ is a coordinate in the phase space, which lies either on or within the unit sphere, while $u_0 = \sqrt{1 - |\mathbf{u}|^2}$. Our previous example $\mathbf{S} \propto \boldsymbol{\sigma}_z$ corresponds to $\mathbf{u} = (0, 0, 1)$, i.e. the north pole of the unit sphere. By varying the geometric parameters of the structure continuously, one obtains a continuous trajectory in the phase space. Here, we keep the periodicity, thickness and permittivity constant, the other geometrical parameters are optimized variables. In principle, any desired trajectory could be obtained by morphing the designed structure with optimization. As an example, we morph the parallelogram in the previous example. The symmetry ensures $\Delta\varphi_r = 0$ corresponding to trajectories on the $u_1 - u_3$ plane, i.e. requiring two geometric parameters, chosen as α (intersection angle) and a (width) to obtain a desired trajectory. Figure 2(a) and (c) plot the resultant $|r|$ and $\Delta\varphi_t$ as color maps against these two parameters (inset show definitions). Now, we walk along the $|r| = 0$ contour (dashed line in Fig. 2(a)) from $\alpha = 90°$ to 45°. As a result, $\Delta\varphi_t$ decreases from 0 to $-\pi$, with details shown in Fig. 2(b). It corresponds to a trajectory in the SU(2) phase space from the origin (**I** operation) to the north pole ($\boldsymbol{\sigma}_z$ operation), shown as blue dots in Fig. 3(a), and is given by

$$\mathbf{U} = \cos\left(\frac{\Delta\varphi_t}{2}\right)\mathbf{I} + i\sin\left(\frac{\Delta\varphi_t}{2}\right)\boldsymbol{\sigma}_z. \tag{5}$$

We note that a $\mathbf{M}_z$ operation on the structure flips the sign of $\Delta\varphi_t$, reversing the phase space trajectory from the origin to the south-pole. Similarly, for the contour $\Delta\varphi_t = -\pi$ (dashed line in Fig. 2(c)), the resultant $|r|$ varied from 1 to 0 when α varies from 90° to 45°. The corresponding phase space trajectory (red dots in Fig. 3(a)) is on a unit circle on the $u_1 - u_3$ plane from $\boldsymbol{\sigma}_x$ to $\boldsymbol{\sigma}_z$. This family of operations is given by

$$\mathbf{U} = -i|r|\boldsymbol{\sigma}_x - i\sqrt{1 - |r|^2}\boldsymbol{\sigma}_z. \tag{6}$$

Equation (6) can also be written as

$$\mathbf{U} = -i\begin{pmatrix} \sqrt{1 - |r|^2} & -|r| \\ |r| & \sqrt{1 - |r|^2} \end{pmatrix}\begin{pmatrix} 1 & 0 \\ 0 & -1 \end{pmatrix}. \tag{7}$$

Physically, this hybrid transformation can be generated by a combination of a beam splitter with unequal reflectance/transmittance and a π phase shifter only at one port. Here such transformation can be implemented by one single layer metasurface. To complete the trajectory going from $\boldsymbol{\sigma}_x$ to **I** along the u_1 axis, we vary the width a of the rectangle ($\alpha = \pi/2$) in Fig. 2(a) and (c) and plotted the phase space trajectory with green dots in Fig. 3(a). This family of operations is given

Optics EXPRESS

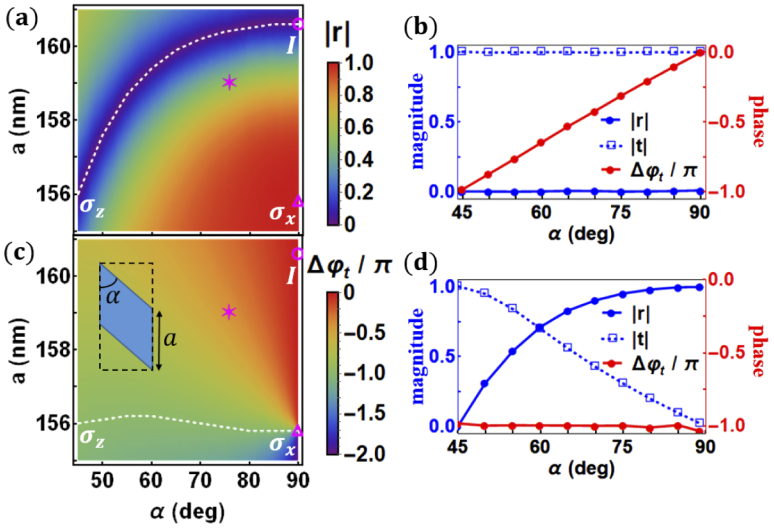

Fig. 2. Scanning two geometric parameters (α, a) of the parallelogram to obtain trajectories in the SU(2) phase space: (a, b) along the u_3-axis by keeping $|r| = 0$ and (c, d) the unit circle in the u_1-u_3 plane by keeping $\Delta\varphi_t = -\pi$. The suitable parameters for the desired transformation are on the dashed line, and the corresponding scattering properties are displayed in the (b) and (d). A closed path $\mathbf{I} \rightarrow \boldsymbol{\sigma}_z \rightarrow \boldsymbol{\sigma}_x \rightarrow \mathbf{I}$ in parameter space corresponds to a closed path in the SU(2) phase space. The geometric parameters of an operation represent by the star symbol (see Fig. 3(a)) can be located.

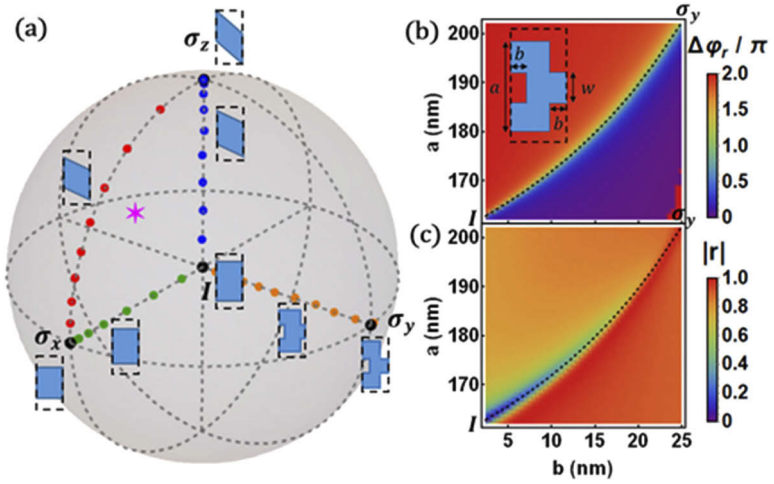

Fig. 3. (a) Implementing various unitary transformation in the SU(2) phase space with various structures. The evolution trajectory is displayed by various color scatters. A particular point (star symbol) in phase-space can be mapped to structure parameters in Fig. 2(a, c). (b, c) The trajectory along the u_2-axis is obtained by optimizing the reflection phase difference and reflection amplitude in the parameters space. The suitable parameters are parameters on the dashed line, with constant $w = 47.5$ nm. The $\boldsymbol{\sigma}_y$ operation is located at $(b, a) = (25.0, 202.1)$ nm.

Optics EXPRESS

by

$$\mathbf{U} = \sqrt{1-|r|^2}\mathbf{I} - i|r|\boldsymbol{\sigma}_x. \tag{8}$$

Now we have a plane enclosed by these three paths in the phase space, any point on this plane is also accessible by morphing the designed structure. To realize this we choose a point marked by a star symbol in Fig. 3(a), and the corresponding structure parameters can be located by reading Fig. 2(a, c).

We have demonstrated the principle to obtain a desired unitary transformation by morphing the geometric configuration of our structure. Up to now, we have investigated the u_1 and u_3 components in the phase space. In fact, it is also possible to add a u_2 component (need $\Delta\varphi_r \neq 0$) by further breaking $\mathbf{M}_z$ and $\mathbf{P}$ symmetry. As an example, we consider a family of "bulge-pit" structures shown in the inset in Fig. 3(b) and located a point corresponds to the $\boldsymbol{\sigma}_y$ operation with geometric parameters found in the caption in Fig. 3. The proposed structure is compatible with the previous parallelogram/rectangle design and can be continuously morphed among each other. The phase space trajectory from $\mathbf{I}$ to $\boldsymbol{\sigma}_y$ along the u_2 axis is generated by preserving $\mathbf{M}_x$ symmetry to keep $\Delta\varphi_t = 0 (u_3 = 0)$ and allow $\Delta\varphi_r \neq 0 (u_2 \neq 0)$. Here, we select two geometric parameters (b, a) to construct this unitary transformation, while the width of the bulge/pit, w, is constant. Along the dashed line in Fig. 3(b)/(c), we see that $\Delta\varphi_r = \pi$ and $|r|$ varied from 0 to 1, as our desired family of operations

$$\mathbf{U} = \sqrt{1-|r|^2}\mathbf{I} - i|r|\boldsymbol{\sigma}_y. \tag{9}$$

Again, a $\mathbf{M}_z$ operation on the structure allows us to walk from $(0, 0, 0)$ to $(0, -1, 0)$ along the u_2 axis.

Next, we turn to the discussion of U(4). Figure 4(a) shows the conventional optical implementation by cascading into six U(2) elements, using a network of beam splitters and phase shifters with 4 ports [4]. The working principle of the discussed metasurface could be extended to control 2 or more qubits based on the additional degree of freedom of photon. By adding the polarization degree of freedom, the scattering matrix extends to the class of U(4) transformation. The photonic state is now written as

$$|\psi\rangle = E_{\mathrm{V},1}|0,0\rangle + E_{\mathrm{V},2}|0,1\rangle + E_{\mathrm{H},1}|1,0\rangle + E_{\mathrm{H},2}|1,1\rangle \tag{10}$$

where for the computational basis $|i, j\rangle$, the polarization qubit is denoted in the first index with $i = 0(1)$ for vertical (horizontal) polarization, and the path qubit is denoted in the second index with $j = 0(1)$ for the beam 1(2). The 4×4 unitary scattering matrix connects the input and output states via

$$\begin{pmatrix} E_{\mathrm{V},1}^{(\mathrm{out})} \\ E_{\mathrm{V},2}^{(\mathrm{out})} \\ E_{H,1}^{(\mathrm{out})} \\ E_{\mathrm{H},2}^{(\mathrm{out})} \end{pmatrix} = \mathbf{S} \begin{pmatrix} E_{\mathrm{V},1}^{(\mathrm{in})} \\ E_{\mathrm{V},2}^{(\mathrm{in})} \\ E_{H,1}^{(\mathrm{in})} \\ E_{H,2}^{(\mathrm{in})} \end{pmatrix} \tag{11}$$

As usual $\mathbf{S}$ is defined as reference to the middle-plane ($z = 0$) of the metasurface and any global phase factor can be ignored. In the single-photon language, we can replace the mode function $\mathbf{E}$ with the mode (annihilation) operator $\hat{\mathbf{a}}$ in Eq. (11) [34]. Here, using the polarization qubit as control and path qubit as target, we can simulate a family of single-photon two-qubit controlled-U-like operations. Figure 4(a) shows our design as a square array of silicon rods with on-plane rotational angle β. In this setting there is no polarization conversion due to $\mathbf{M}_y$

Optics EXPRESS

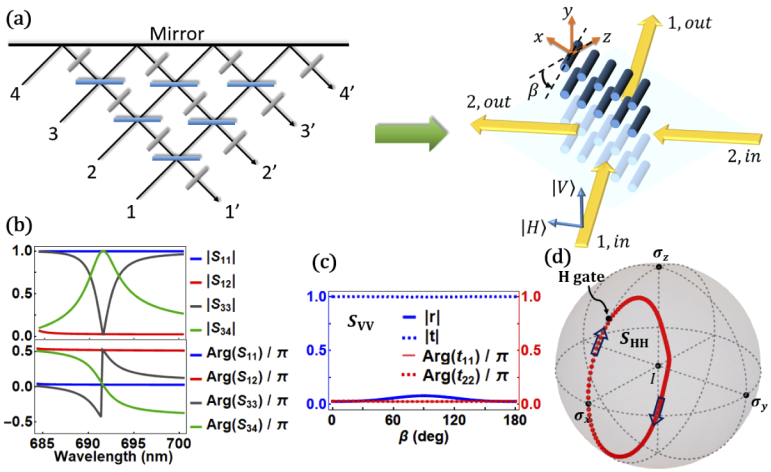

Fig. 4. The CNOT-gate-like operation as typical examples of U(4) implementations. (a) Metasurface for U(4) implementation to simplify conventional implementation which require cascading into network of beam splitters (blue rectangle) and phase shifters (grey rectangle) with 4 ports. The metasurface consists of an array of dielectric rods with on-plane rotation β. Oblique incidence is set on both sides at 45 degree, vertical polarization is defined in the y direction and horizontal polarization is defined on the incident x-z plane. (b) Resonance to obtain CNOT gate (at $\beta = 0$) with unit vertical and zero horizontal polarization transmittance. (c) **S** matrix for vertical polarization approximates a 2×2 identity operation as β varies. (d) Trajectory in the reduced SU(2) phase-space for horizontal polarization when β varies from 0 to π (along the direction of arrow). Controlled-H-like operation is simulated at $\beta = 15°$. Structure parameters: dielectric ($\varepsilon_r = 12$) rods with radius 30 nm, length 360 nm and lattice constant 400 nm.

symmetry and the scattering matrix is in a simple block form

$$\mathbf{S} = \begin{pmatrix} \mathbf{S}_{\mathrm{VV}} & 0 \\ 0 & \mathbf{S}_{\mathrm{HH}} \end{pmatrix} \xrightarrow{\beta=0} \begin{pmatrix} \mathbf{I} & 0 \\ 0 & \boldsymbol{\sigma}_x \end{pmatrix}, \tag{12}$$

approaching our targeting CNOT-like operation when $\beta = 0$ [23,41]. Detailed geometric parameters can be found in the caption of Fig. 4. At the operational wavelength of 685 nm and $\beta = 0$, an electric resonance occurs (excited by the normal component of electric field E_z). The resonance results perfect reflectance in horizontal polarization (**E**-field on x-z plane): a value of nearly zero for $S_{33}(= S_{44})$ and a value of nearly one for $S_{34}(= S_{43})$. On the other hand, the structures do not respond resonantly to vertically polarized light (E-field along y) to have nearly unit transmittance: value one for $S_{11}(= S_{22})$ and value 0 for $S_{12}(= S_{21})$. We note that the phase of S_{11} and S_{34} are found to be equal at the operational wavelength, as shown in Fig. 4(b). Due to the small dimension of the rod radius, we expect the vertically polarized light give little respond ($\mathbf{S}_{\mathrm{VV}} = \mathbf{I}$) upon on-plane rotation of the rods, this morphing of structure would only modify the respond in horizontal polarization which alone satisfies the unitary condition $\mathbf{S}_{\mathrm{HH}}\mathbf{S}_{\mathrm{HH}}^{\dagger} = \mathbf{I}$, simulating a family of controlled-U-like operations. While having a CNOT-gate-like operation at $\beta = 0$ as a starting point, varying β from 0 to π gives a continuous and closed trajectory in the SU(4) phase space. Figure 4(c) shows our assertion that slight influence on the evolution in the vertical polarization channel. Then the description can be simplified using a reduced SU(2) phase space for the horizontal polarization channel. This evolution trajectory is plotted in Fig. 4(d) which lies on the u_1-u_3 plane, as we continuously vary β. This verifies the single-photon

Optics EXPRESS

two-qubit U(4) operation by adding the polarization degree of freedom of photon with the designed metasurfaces. As a particular example, controlled-H-like operation is simulated at $\beta = 15°$.

Further by considering the out-of-plane rotation ($\alpha \neq 0$) of the dielectric rods (see Fig. 5(a)), vertical and horizontal polarization channels are coupled and an U(4) operation with non-zero off-diagonal block in Eq. (12) can be generalized. We write the SU(4) scattering matrix as

$$\mathbf{U} = \exp\left(-i \sum_{\substack{i,j=0 \\ \{i,j\}\neq\{0,0\}}}^{3} s_{ij}\boldsymbol{\sigma}_i \otimes \boldsymbol{\sigma}_j\right) = \mathbf{K}_1 \exp\left(\frac{i}{2}\sum_{i=1}^{3}\theta_i \boldsymbol{\sigma}_i \otimes \boldsymbol{\sigma}_i\right)\mathbf{K}_2, \tag{13}$$

where the first equality shows the dependence on 15 real numbers s_{ij} for any SU(4) matrix, and $(\boldsymbol{\sigma}_0, \boldsymbol{\sigma}_1, \boldsymbol{\sigma}_2, \boldsymbol{\sigma}_3) = (\mathbf{I}, \boldsymbol{\sigma}_x, \boldsymbol{\sigma}_y, \boldsymbol{\sigma}_z)$. The second equality provides a simpler description for any SU(4) matrix in terms of its non-local part with 3 real numbers θ_i, here $\mathbf{K}_{1,2} \in \mathrm{SU}(2) \otimes \mathrm{SU}(2)$ is a local unitary operation [42]. First, we rotate the rods on the y-z plane ($\beta = 0$). We plot the 5 non-zero s_{ij} in Fig. 5(b) as α varies. Next, we investigate the general case with both α and β being non-zero. The non-local part of $\mathbf{U}$ is described by the Weyl chamber, where the parameter space $(\theta_1, \theta_2, \theta_3)$ is a tetrahedron $\mathrm{OA_1A_2A_3}$, the line OL represent all the controlled-U operations and the point L is the CNOT gate [42]. As we vary α and β from 0 to π, the θ-parameters lie on the slanted surface $\mathrm{OA_1A_3}$, as shown in Fig. 5(c) with the blue dots. The $\alpha = 0$ contour (red line) coincides with the line OL, showing that all controlled-U operations are obtained apart from a local unitary transformation $\mathbf{K}_{1,2}$, in the single-photon two-qubit context. For non-zero α (such as the $\beta = 0$ contour, green line in Fig. 5(c)), the trajectory escape the line OL which shows more general SU(4) operations other than the controlled-U subset.

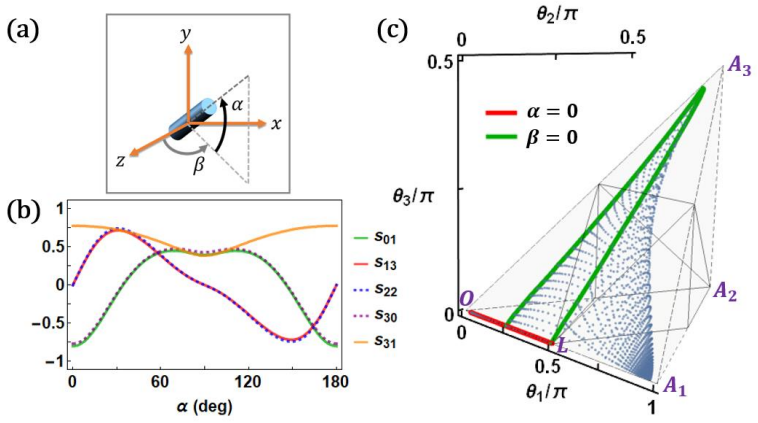

Fig. 5. (a) Orientation of the dielectric rods for the metasurface in Fig. 4(a), the incident plane (x-z plane) defines the on-plane rotation β and the off-plane rotation α. (b) The SU(4) scattering matrix is described by 15 real numbers (see Eq. (13)). The non-zero s_{ij} are plotted with varying α and $\beta = 0$. (c) The non-local part of the SU(4) scattering matrix is plotted in the Weyl chamber as blue dots, with α and β vary from 0 to π. Point L is the CNOT operation at $\alpha = \beta = 0$. Red line shows the $\alpha = 0$ contour, coincides with line OL that represent all controlled-U operations. Green line shows the $\beta = 0$ contour which gives more general SU(4) operations other than the controlled-U subset.

Although these single-photon two-qubit operations are not scalable for universal quantum computation, they can be applied for single-photon few-qubit quantum information processing [43]. The above metasurface can be potentially useful to simplify or replace some of the U(4)

Optics EXPRESS

operations within a specific quantum gate originally constructed from conventional optical elements. One example is a non-linear sign gate, using only linear optical elements with ancilla photons and post-selection, which can be applied in the KLM quantum computation protocol [44]. To generalize to larger number of qubit operation, the usual decomposition into multiport network of U(2) elements [4] is not favorable due to the propagation loss originated from the long optical depth (see Fig. 4(a)). Improved multiport network [45] has been studied for this purpose to reduce the optical depth. However, if factorization scheme is available, decomposition into multiport network of our U(4) metasurface elements can help significantly reduce optical depth and propagation loss. Finally, by introducing more than one incident photon to the metasurface, two- or multi-photon interference effect can be studied and provide potential application, such as quantum state preparation.

3. Discussion and conclusion

Benefit from the metasurfaces with structure design freedom, we theoretically construct a suite of element unitary transformations, which composes the general U(2) transformation on a photonic qubit. By adding the polarization degree of freedom, U(4) transformation can also be implemented, a CNOT-like gate, a family of controlled-U-like and other U(4) operations are numerically demonstrated as examples of deterministic single-photon two-qubit operations. These theoretical verifications clearly show that the metasurface approach can be potential candidate substituting the conventional linear optical elements to generate designer unitary transformations in the future few-qubit quantum information processing protocols with more integrated feasibility.

Funding. Research Grants Council, University Grants Committee of Hong Kong (16303019, 16303417, 16304520); National Natural Science Foundation of China (11974259).

Disclosures. The authors declare no conflicts of interest.

References

1. M. A. Nielsen and I. L. Chuang, *Quantum Computation and Quantum Information* (Cambridge University, 2000).
2. P. Kok, W. J. Munro, K. Nemoto, T. C. Ralph, J. P. Dowling, and G. J. Milburn, "Linear optical quantum computing with photonic qubits," Rev. Mod. Phys. **79**(1), 135–174 (2007).
3. J. L. O'Brien, "Optical quantum computing," Science **318**(5856), 1567–1570 (2007).
4. M. Reck, A. Zeilinger, H. J. Bernstein, and P. Bertani, "Experimental realization of any discrete unitary operator," Phys. Rev. Lett. **73**(1), 58–61 (1994).
5. N. Tischler, C. Rockstuhl, and K. Słowik, "Quantum optical realization of arbitrary linear transformations allowing for loss and gain," Phys. Rev. X **8**(2), 021017 (2018).
6. A. A. Melnikov, H. P. Nautrup, M. Krenn, V. Dunjko, M. Tiersch, A. Zeilinger, and H. J. Briegel, "Active learning machine learns to create new quantum experiments," Proc. Natl. Acad. Sci. U. S. A. **115**(6), 1221–1226 (2018).
7. N. Yu and F. Capasso, "Flat optics with designer metasurfaces," Nat. Mater. **13**(2), 139–150 (2014).
8. S. B. Glybovski, S. A. Tretyakov, P. A. Belov, Y. S. Kivshar, and C. R. Simovski, "Metasurfaces: From microwaves to visible," Phys. Rep. **634**, 1–72 (2016).
9. X. Ni, A. V. Kildishev, and V. M. Shalaev, "Metasurface holograms for visible light," Nat. Commun. **4**(1), 2807 (2013).
10. L. Huang, X. Chen, H. Mühlenbernd, H. Zhang, S. Chen, B. Bai, Q. Tan, G. Jin, K.-W. Cheah, C.-W. Qiu, J. Li, T. Zentgraf, and S. Zhang, "Three-dimensional optical holography using a plasmonic metasurface," Nat. Commun. **4**(1), 2808 (2013).
11. F. Aieta, M. A. Kats, P. Genevet, and F. Capasso, "Multiwavelength achromatic metasurfaces by dispersive phase compensation," Science **347**(6228), 1342–1345 (2015).
12. M. Khorasaninejad and F. Capasso, "Metalenses: Versatile multifunctional photonic components," Science **358**(6367), eaam8100 (2017).
13. S. Xiao, F. Zhong, H. Liu, S. Zhu, and J. Li, "Flexible coherent control of plasmonic spin-Hall effect," Nat. Commun. **6**(1), 8360 (2015).
14. J. P. Balthasar Mueller, K. Leosson, and F. Capasso, "Ultracompact metasurface in-line polarimeter," Optica **3**(1), 42–47 (2016).
15. E. Arbabi, S. M. Kamali, A. Arbabi, and A. Faraon, "Full-Stokes imaging polarimetry using dielectric metasurfaces," ACS Photonics **5**(8), 3132–3140 (2018).

Optics EXPRESS

16. A. Silva, F. Monticone, G. Castaldi, V. Galdi, A. Alù, and N. Engheta, "Performing Mathematical Operations with Metamaterials," Science **343**(6167), 160–163 (2014).
17. T. Zhu, Y. Zhou, Y. Lou, H. Ye, M. Qiu, Z. Ruan, and S. Fan, "Plasmonic computing of spatial differentiation," Nat. Commun. **8**(1), 15391 (2017).
18. H. Kwon, D. Sounas, A. Cordaro, A. Polman, and A. Alù, "Nonlocal Metasurfaces for optical signal processing," Phys. Rev. Lett. **121**(17), 173004 (2018).
19. C. Della Giovampaola and N. Engheta, "Digital metamaterials," Nat. Mater. **13**(12), 1115–1121 (2014).
20. N. M. Estakhri, B. Edwards, and N. Engheta, "Inverse-designed metastructures that solve equations," Science **363**(6433), 1333–1338 (2019).
21. T. J. Cui, M. Q. Qi, X. Wan, J. Zhao, and Q. Chen, "Coding metamaterials, digital metamaterials and programmable metamaterials," Light: Sci. Appl. **3**(10), e218 (2014).
22. T. J. Cui, S. Liu, and L. L. Li, "Information entropy of coding metasurface," Light: Sci. Appl. **5**(11), e16172 (2016).
23. M. Fiorentino and F. N. C. Wong, "Deterministic controlled-NOT gate for single-photon two-qubit quantum logic," Phys. Rev. Lett. **93**(7), 070502 (2004).
24. K. H. Kagalwala, G. Di Giuseppe, A. F. Abouraddy, and B. E. Saleh, "Single-photon three-qubit quantum logic using spatial light modulators," Nat. Commun. **8**(1), 739 (2017).
25. E. Knill, R. Laflamme, and G. L. Milburn, "A scheme for efficient quantum computation with linear optics," Nature (London, U. K.) **409**(6816), 46–52 (2001).
26. E. Altewischer, M. P. van Exter, and J. P. Woerdman, "Plasmon-assisted transmission of entangled photons," Nature (London, U. K.) **418**(6895), 304–306 (2002).
27. M. Siomau, A. A. Kamli, S. A. Moiseev, and B. C. Sanders, "Entanglement creation with negative index metamaterials," Phys. Rev. A: At., Mol., Opt. Phys. **85**(5), 050303 (2012).
28. P. K. Jha, N. Shitrit, J. Kim, X. Ren, Y. Wang, and X. Zhang, "Metasurface-Mediated Quantum Entanglement," ACS Photonics **5**(3), 971–976 (2018).
29. T. Stav, A. Faerman, E. Maguid, D. Oren, V. Kleiner, E. Hasman, and M. Segev, "Quantum entanglement of the spin and orbital angular momentum of photons using metamaterials," Science **361**(6407), 1101–1104 (2018).
30. P. K. Jha, X. Ni, C. Wu, Y. Wang, and X. Zhang, "Metasurface-enabled remote quantum interference," Phys. Rev. Lett. **115**(2), 025501 (2015).
31. T. Roger, S. Vezzoli, E. Bolduc, J. Valente, J. J. F. Heitz, J. Jeffers, C. Soci, J. Leach, C. Couteau, N. I. Zheludev, and D. Faccio, "Coherent perfect absorption in deeply subwavelength films in the single-photon regime," Nat. Commun. **6**(1), 7031 (2015).
32. K. Wang, J. G. Titchener, S. S. Kruk, L. Xu, H.-P. Chung, M. Parry, I. Kravchenko, Y.-H. Chen, A. S. Solntsev, Y. S. Kivshar, D. N. Neshev, and A. A. Sukhorukov, "Quantum metasurface for multi-photon interference and state reconstruction," Science **361**(6407), 1104–1108 (2018).
33. L. Li, Z. Liu, X. Ren, S. Wang, V. C. Su, M. K. Chen, C. H. Chu, H. Y. Kuo, B. Liu, W. Zang, G. Guo, L. Zhang, Z. Wang, S. Zhu, and D. P. Tsai, "Metalens-array–based high-dimensional and multiphoton quantum source," Science **368**(6498), 1487–1490 (2020).
34. Y. D. Chong, L. Ge, H. Cao, and A. D. Stone, "Coherent perfect absorbers: Time-reversed lasers," Phys. Rev. Lett. **105**(5), 053901 (2010).
35. J. Zhang, K. F. MacDonald, and N. I. Zheludev, "Controlling light-with-light without nonlinearity," Light: Sci. Appl. **1**(7), e18 (2012).
36. U. Leonhardt, "Quantum physics of simple optical instruments," Rep. Prog. Phys. **66**(7), 1207–1249 (2003).
37. W. Suh, Z. Wang, and S. Fan, "Temporal coupled-mode theory and the presence of non-orthogonal modes in lossless multimode cavities," IEEE J. Quantum Electron. **40**(10), 1511–1518 (2004).
38. S. Fan, W. Suh, and J. D. Joannopoulos, "Temporal coupled-mode theory for the Fano resonance in optical resonators," J. Opt. Soc. Am. A **20**(3), 569–572 (2003).
39. K. X. Wang, Z. Yu, S. Sandhu, and S. Fan, "Fundamental bounds on decay rates in asymmetric single-mode optical resonators," Opt. Lett. **38**(2), 100–102 (2013).
40. D. L. Sounas and A. Alù, "Time-reversal symmetry bounds on the electromagnetic response of asymmetric structures," Phys. Rev. Lett. **118**(15), 154302 (2017).
41. S. M. Wang, Q. Q. Cheng, Y. X. Gong, P. Xu, C. Sun, L. Li, T. Li, and S. N. Zhu, "A 14 × 14 μm^2 footprint polarization-encoded quantum controlled-NOT gate based on hybrid waveguide," Nat. Commun. **7**(1), 11490 (2016).
42. J. Zhang, J. Vala, S. Sastry, and K. B. Whaley, "Geometric theory of nonlocal two-qubit operations," Phys. Rev. A **67**(4), 042313 (2003).
43. N. J. Cerf, C. Adami, and P. G. Kwiat, "Optical simulation of quantum logic," Phys. Rev. A **57**(3), R1477–R1480 (1998).
44. T. Rudolph and J.-W. Pan, "A simple gate for linear optics quantum computing," arXiv:quant-ph/0108056.
45. W. R. Clements, P. C. Humphreys, B. J. Metcalf, W. S. Kolthammer, and I. A. Walmsley, "Optimal design for universal multiport interferometers," Optica **3**(12), 1460 (2016).